Check for updates

Proceedings of the ASME 2026 21st International Manufacturing Science and Engineering Conference
MSEC2026
June 14–18, 2026, State College, Pennsylvania

MSEC2026-182587

Downloaded from asmedigitalcollection.asme.org/MSEC/proceedings-pdf/MSEC2026/89633/V002T05A011/7651958/v002t05a011-msec2026-182587.pdf by Purdue University at West Lafayette, Yuseop Sim on 05 November 2026

COLD SPRAY DEPOSITION OF LUNAR REGOLITH COMPOSITE POWDERS TOWARDS IN-SPACE ELECTRONICS MANUFACTURING

Sazedur Rahman[1], Semih Akin [1,*]

[1]Department of Mechanical, Aerospace and Nuclear Engineering, Rensselaer Polytechnic Institute, Troy, NY 12180, USA

ABSTRACT

In-space manufacturing and in-situ resource utilization (ISRU) are essential for sustainable space exploration, reducing mission costs and dependence on Earth-supplied resources. To realize this vision, it is vital to develop methods for fabricating structural and electronic components from locally available lunar regolith. This study employs the cold spray (CS) particle deposition, utilizing engineered lunar regolith composite feedstocks to fabricate electrically conductive coatings under terrestrial conditions. In this regard, composite powders are produced by ball-milling lunar regolith simulant (LHS-1D) with ductile metallic (Sn) additives, followed by cold spray deposition onto a PEEK (polyether ether ketone) substrate (i.e., a space-grade polymer known for its outstanding mechanical strength and thermal stability). The effect of lunar regolith content (i.e., ranging from 50 to 80 wt%) on the conductivity of developed coatings is comprehensively investigated through detailed microstructural and electrical analyses. Moreover, the high-strain-rate finite element simulations are conducted to elucidate the particle impact dynamics and deposition mechanisms during CS. The fabricated coatings exhibit tunable electrical performance (1500 – 3300 $S.cm^{-1}$) depending on metallic loading, along with promising adhesion strength (7.30 – 8.46 MPa). Experimental demonstrations—including circuit deposition and flexible electronics validated the feasibility of the CS process for achieving regolith-based conductive coating with promising reliability and durability. Collectively, this work establishes a foundation for solid-state CS deposition of lunar regolith-based electronics, underscoring its distinct advantages for future lunar missions and offering a promising pathway toward in-space electronics manufacturing.

Keywords: Space manufacturing, electronics, in-situ resource utilization (ISRU), cold spray additive manufacturing (CSAM), lunar regolith, LHS-1D, composite powder

NOMENCLATURE

Roman letters

A	Initial flow stress [MPa]
A'	Cross-sectional area [m^2]
B	Pre-exponential factor [MPa]
C	Strain rate factor
E	Young's modulus [GPa]
k	Thermal conductivity [W/m.K]
L	Coating length [m]
m	Thermal softening exponent
n	Work hardening exponent
R	Resistance [Ω]
R_o	Initial resistance [Ω]
T_m	Melting temperature [^oC]
T_o	Refernce temperature [^oC]
t	Coating thickness [μm]
w	Coating width [m]

Greek letters

$\dot{\varepsilon}_0$	Reference strain rate
σ	Equivalent flow stress [MPa]
σ'	Conductivity [S/cm]
ρ	Density [kg/m^3]
ρ'	Resistivity [Ωm]
ν	Poisson's ratio

Abbreviations

AM	Additive Manufacturing
ASTM	American Society for Testing and Materials
CS	Cold Spray
CSAM	Cold Spray Additive Manufacturing
EDX	Energy Dispersive X-ray Spectroscopy
ISRU	In-Situ Resource Utilization
JC	Johnson-Cook
LHS	Lunar Regolith Simulant
PEEK	Polyetheretherketone
PET	Polyethylene Terephthalate
SEM	Scanning Electron Microscope
TPU	Thermoplastic Polyurethane

*Corresponding author: akins@rpi.edu

Copyright © 2026 by ASME

1. INTRODUCTION

The establishment of sustainable lunar infrastructures requires the development of in-situ resource utilization (ISRU) to fabricate structural and functional components directly from local materials [1]. Among these functional needs, the ability to manufacture electronic systems and conductive surfaces is particularly critical for establishing autonomous operations, smart sensing platforms, and energy harvesting systems essential to long-term lunar missions [2]. In this context, lunar regolith (i.e., the fine particulate layer covering the Moon's surface) represents an abundant and versatile feedstock for such applications. Owing to its rich composition of oxides of silicon, aluminum, iron, and titanium [3], regolith can serve as a base material for structural components, radiation shielding, and functional devices such as sensors, energy harvesters, and electronic elements [4].

To harness the potential of lunar regolith, researchers are increasingly employing additive manufacturing (AM) technologies for their ability to enable on-demand fabrication of components and structures [5]. Techniques such as laser powder bed fusion [6], laser-directed energy deposition [7], and material extrusion [8] have been investigated to convert lunar regolith simulant into functional components. However, the extreme vacuum (i.e., $\sim 10^{-12}$ torr (night) to $\sim 10^{-10}$ torr (day) [9]), severe temperature fluctuations [10], and microgravity [11] conditions present challenges for conventional AM processes. In particular, phase-change-based AM techniques are highly susceptible to rapid material evaporation or vaporization under extreme vacuum conditions [12]. Consequently, their implementation on the lunar surface would require a pressurized enclosure, which greatly limits their practicality for on-site, in-situ manufacturing. In contrast, solid-state AM techniques, which operate without melting, offer a promising alternative capable of functioning effectively under reduced-pressure conditions.

Most recently, the authors of this work employed solid-state cold spray (CS) process to deposit regolith simulant powders (LHS-1D) onto space-grade PTFE and investigated the resulting process–structure–property relationships [13]. However, the electrically insulating nature of pure regolith limits its applicability in space applications, including dust mitigation, EMI shielding, electronic devices, energy harvesting-systems etc. —all of which are critical for future lunar missions. To address this, the present study employs the CS process to fabricate electrically conductive coatings under terrestrial conditions using engineered lunar regolith–based composite powder feedstock (see Fig 1a).

First, lunar regolith simulant powders (LHS-1D) are mechanically alloyed with metallic additives (Sn + Al_2O_3) via ball milling at various regolith weight ratios to produce composite feedstocks for the CS process. Next, the synthesized powders are cold sprayed onto polyether ether ketone (PEEK) substrates to fabricate electrically conductive surfaces, with the CS processing parameters guided by particle impact modeling studies. PEEK was selected as the substrate due to its lightweight nature, high thermal stability, and strong mechanical performance, making it well-suited for space and aerospace applications [14]. In parallel, the CS process was evaluated across different polymer systems (i.e., PET and TPU) to assess its versatility and substrate compatibility. Lastly, the fabricated coatings are thoroughly characterized in terms of their microstructure, surface morphology, electrical conductivity, and durability to provide comprehensive assessment of their structural integrity and functional performance.

This study advances the existing body of knowledge in this domain by introducing the following key innovations:

(i) Development of lunar regolith simulant–based composite powders as novel feedstock for the CS process.

(ii) Integration of particle impact modeling to guide the CS process and elucidate deposition dynamics.

(iii) Fabrication of electrically conductive coatings on various polymer substrates, demonstrating potential for in-space electronics manufacturing.

(iv) Comprehensive characterization of CS-fabricated coatings to establish structure–property–performance relationships.

2. MATERIALS AND METHODS

2.1. Materials and powder engineering

Lunar regolith simulant powders (LHS-1D) were procured from *Space Resource Technologies, USA* to use them as the feedstock material for the CS deposition process. LHS-1D is specifically engineered to replicate the composition and physical properties of lunar highland soils [3]. The composition of LHS-1D lunar regolith simulant consists of SiO_2 (49.12%), TiO_2 (0.63%), Al_2O_3 (26.29%), FeO (3.20%), MnO (0.06%), MgO (2.86%), CaO (13.52%), Na_2O (2.55%), K_2O (0.34%), P_2O_5 (0.17%), and LOI (0.41%) [3]. The morphology of the LHS-1D simulant is shown in Fig. 1b, exhibiting a particle size distribution ranging from 0.04 to 35 µm, with a mean diameter of ≈ 7 µm) [3]. Note that the terms "lunar regolith simulant" and "lunar regolith" are used interchangeably throughout this study.

To develop engineered composite powders for the fabrication of electrically conductive coatings, commercial blended metal additive powders (*Titomic, Inc.*) consisting of ductile tin (Sn: 55-45 wt%) and metal-oxide (Al_2O_3: 45-55 wt%) with a mean diameter of ≈ 12 µm (see Fig. 1c) were incorporated into the regolith matrix via ball-milling at various weight ratios (i.e., 20–50 wt%). In this blended powder, the Sn component provides the electrical conductivity, while ceramic (Al_2O_3) content enhances deposition efficiency. Moreover, because lunar regolith naturally contains significant amount Al_2O_3 (26.29%), the overall powder composition aligns with future ISRU pathways and enhances the use of in-situ–relevant materials.

Ball milling was performed using a planetary ball mill (*Across International*). The process was carried out at a rotational speed of 220 rpm for 4 hours, with a powder-to-ball weight ratio of 1:3. Stainless steel balls (6 mm diameter) and jars (capacity 100 ml) were used as the milling media. These parameters were chosen to ensure uniform dispersion of the metal additives within the regolith matrix while minimizing particle fracture and contamination, thereby enabling homogeneous compositional mixing. Moreover, ball milling facilitates mechanical alloying, imparting the required ductility needed to achieve favorable sprayability and reliable deposition performance.

Fig. 1d shows the morphology of the resulting composite powders composed of 50 %wt regolith + 50 %wt Sn + Al_2O_3. The corresponding EDX elemental map in Fig. 1e confirms

Downloaded from asmedigitalcollection.asme.org/MSEC/proceedings-pdf/MSEC2026/89633/V002T05A011/7651958/v002t05a011-msec2026-182587.pdf by Purdue University at West Lafayette, Yuseop Sim on 05 November 2026

Copyright © 2026 by ASME

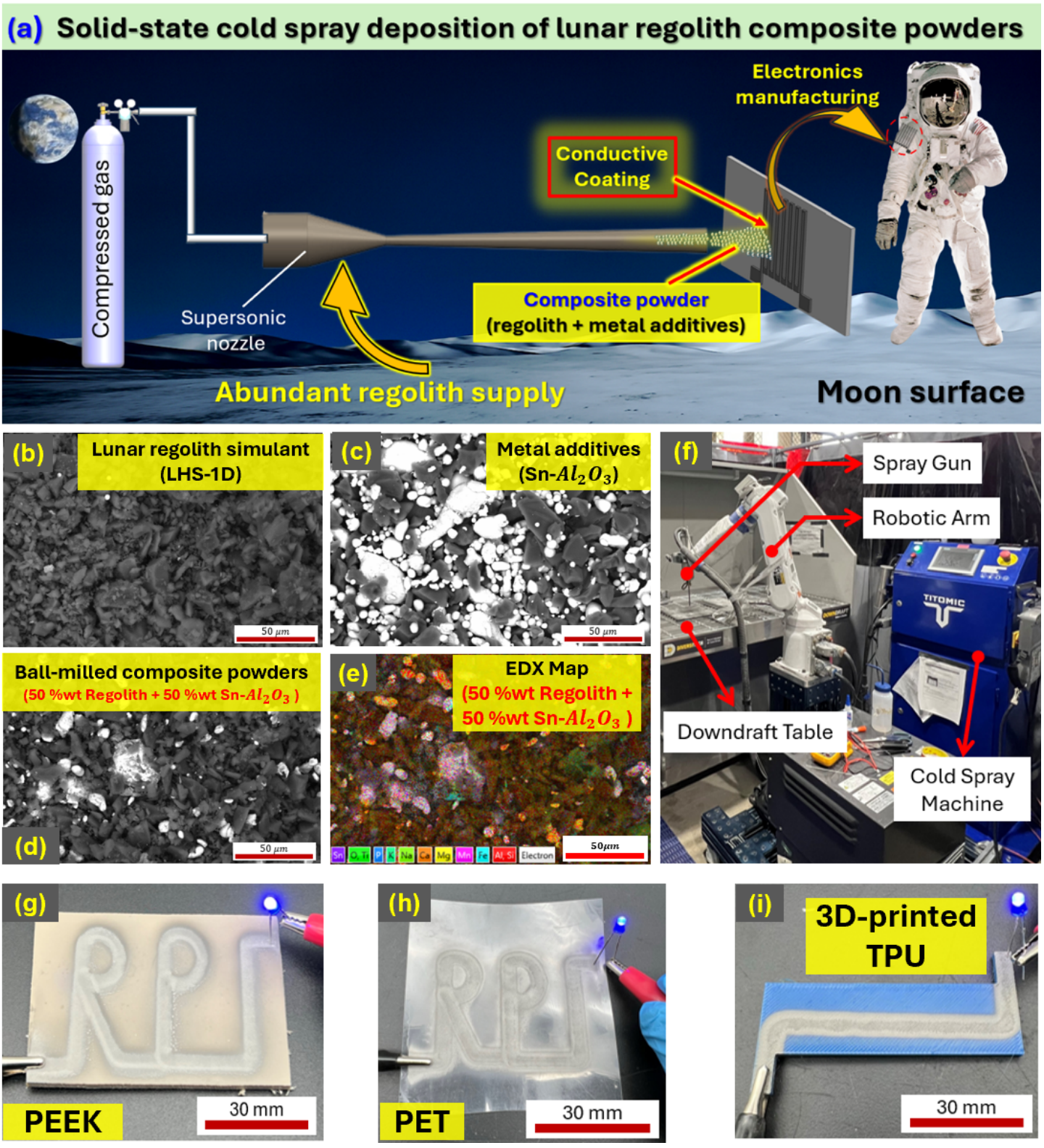


FIGURE 1: Cold spray (CS) deposition of electrically conductive lunar regolith composite coatings: (a) Conceptual illustration of CS-based electronics manufacturing from lunar regolith; (b) Morphology of the lunar regolith simulant (LHS-1D) powders; (c) Morphology of the metal additive powders (Sn + Al_2O_3); (d) Ball-milled composite powders and (e) Corresponding EDX elemental map confirming uniform distribution; (f) Robotic CS experimental setup; Programmable deposition of conductive regolith composite coatings on various polymer substrates: (g) PEEK, (h) PET, and (i) 3D-printed TPU.

Copyright © 2026 by ASME

Downloaded from asmedigitalcollection.asme.org/MSEC/proceedings-pdf/MSEC2026/89633/V002T05A011/7651958/v002t05a011-msec2026-182587.pdf by Purdue University at West Lafayette, Yuseop Sim on 05 November 2026

the distribution of key elements (viz., Sn, Si, Al, Ca, O, Fe, Mg, Ti) within the regolith-metal matrix, indicating successful compositional mixing and the formation of composite feedstock suitable for CS deposition. No contamination from the stainless-steel ball-milling vials or balls was detected, as evidenced by the absence of a chromium peak in the EDX analysis.

As for the substrate material, polyether ether ketone (PEEK) was selected as the primary substrate material due to its extensive use in space-related applications, owing to its excellent mechanical strength, thermal stability, radiation resistance, and low outgassing characteristics [15]. Accordingly, PEEK coupons with dimensions of 30 mm × 20 mm × 3.2 mm were prepared and used without any surface treatment prior to the CS deposition. To further demonstrate the versatility of the approach, the feasibility of CS deposition with lunar regolith composite powders was also evaluated on additional polymeric substrates, including polyethylene terephthalate (PET) and thermoplastic polyurethane (TPU).

2.2. Cold spray deposition

Electrically conductive functional surfaces were deposited onto polymeric substrates using a low-pressure CS system (*Titomic D-523*), equipped with a nozzle mounted on a multi-axis robotic arm (*Yaskawa*), as shown in Fig. 1f. In CS deposition, micron-scale particles (5-100 µm) are propelled through a supersonic nozzle and impact the at high velocity (> 300 m/s), where they undergo plastic deformation and mechanically interlock with the substrate to form a dense coating [16]. The unique characteristics of the CS process—such as its solid-state nature, low processing temperature, and minimal oxidation [17]—make it particularly suitable for depositing heat-sensitive materials, including various polymeric substrates. Figs. 1g-i showcase the programmable CS deposition (writing) of composite powders (50 %wt regolith + 50 %wt metal) onto various polymeric substrates, including PEEK, PET, and TPU, achieving electrically conductive coatings. The CS parameters used in this study were as follows: gas temperature of 300°C, gas pressure of 0.5 MPa, nozzle traverse speed of 25 mm/s, and a constant spray standoff distance of 30 mm. The rationale for selecting these process settings is detailed in Section 3.1.

2.3. Characterization

The microstructure of the coatings was examined using scanning electron microscopy (SEM, *FEI Versa*), and their elemental composition was analyzed via Energy Dispersive X-ray Spectroscopy (EDX). For cross-sectional analysis, specimens were cold-mounted in resin (90% resin, 10% hardener), cured for 24 hours, and sequentially polished with abrasive papers up to 1200 grit, followed by 3 μm and 0.3 μm fine polishing. To minimize charging on the PEEK substrate, samples were sputter-coated with a thin platinum (Pt) layer before imaging. Coating thickness and porosity were quantified from SEM micrographs using *ImageJ*.

The electrical resistance was measured using the two-point probe method with a digital multimeter (*Fluke*). The average resistance values were used to estimate electrical conductivity. Adhesion strength of the coatings was evaluated using the pull-off adhesion test following ASTM D4541 [18], employing an adhesion tester *Elcometer 510*. All characterization tests were performed on at least three specimens for reproducibility.

3. RESULTS AND DISCUSSION

3.1. Cold spray particle impact modeling

A Lagrangian-based single particle impact modeling was developed to: (i) elucidate particle–substrate impact interactions under representative CS processing conditions and (ii) validate the selected process parameters prior to the experimental characterizations presented in the following sections. In particular, ensuring plastic deformation of ductile conductive additives (Sn) upon impact is essential to achieve electrically conductive coatings, as pure regolith and Al_2O_3 phases are inherently insulating. Accordingly, the modeling focused exclusively on Sn particles, allowing us to capture the deformation behavior responsible for bonding and electrical percolation. The brittle Al_2O_3 and regolith constituents were not included, as they do not undergo significant plastic deformation and thus do not govern the conductive pathways in the final coating.

To capture the high-strain-rate deformation behavior during CS impact, the Johnson–Cook (J–C) plasticity model [19] was used. This constitutive model expresses the flow stress as a coupled function of plastic strain, strain rate, and temperature, enabling realistic representation of the severe thermo-mechanical loading experienced by particles upon impact. The J–C model is formulated as follows [20]:

$$\sigma = \left[A + B(\varepsilon_p)^n\right]\left[1 + C\ln\left(\frac{\dot{\varepsilon}_p}{\dot{\varepsilon}_0}\right)\right]\left[1 - (T^*)^m\right] \qquad (1)$$

where σ = equivalent flow stress, ε_p = equivalent plastic strain, $\dot{\varepsilon}_p$ = plastic strain rate, $\dot{\varepsilon}_0$ = reference strain rate, $T^* = (T - T_0)/(T_m - T_0)$ = homologous temperature, and A, B, C, n, m = material constants.

In the simulation, single particle impact was considered, where the particle was modeled as pure tin (Sn) impacting on a PEEK substrate. For simplicity, the J-C model was applied to both the particle and the substrate, neglecting the inherently viscoelastic, rate-dependent, and nonlinear mechanical behavior of polymeric materials. This simplified configuration allows for capturing the particle deformation and interfacial interaction with the polymeric surface without the added complexity [21]. Such a single-impact analysis provides essential insights into the underlying deposition mechanisms and supports the interpretation of experimentally observed deposition patterns [22].

The JC parameters for both the particle (Sn) and the substrate (PEEK) are presented in Table 1, which were adopted from the existing literature. Only the Sn particle was modeled in the single-particle impact analysis, as the formation of a conductive coating is primarily governed by the plastic deformation of Sn. Additionally, the current literature lacks J-C parameters for lunar regolith simulant powders (LHS-1D), further justifying this modeling simplification. The computational domain, along with the relevant boundary conditions (BCs), is illustrated in Fig. 2a.

Downloaded from asmedigitalcollection.asme.org/MSEC/proceedings-pdf/MSEC2026/89633/V002T05A011/7651958/v002t05a011-msec2026-182587.pdf by Purdue University at West Lafayette, Yuseop Sim on 05 November 2026

Copyright © 2026 by ASME

An axisymmetric BC was applied to reflect the inherent symmetry of the geometry. The bottom surface of the PEEK substrate was fixed and maintained at room temperature (298 K), while the lateral surfaces were assigned symmetry conditions. For the inlet boundary conditions, the Sn particle temperature (473 K) and impact velocity (330 m/s) were adopted from [23]. In that study, these particle conditions were obtained under representative CS processing parameters, specifically a gas temperature of 300°C and a gas pressure of 0.5 MPa. These CS settings are also consistent with those used to successfully deposit regolith onto PTFE films in our previous work [13].

Fig. 2b shows the FE mesh, featuring a refined element size of 1 µm across the domain. The Coulomb friction model was used to capture interfacial interactions between the particle and the substrate, with the friction coefficient set to 0.1. In addition, the selected CS process parameters were compared with the authors' recently published work [13] on cold spraying of pure regolith on a polymeric substrate to confirm the successful deposition of regolith–Sn composite particles on a PEEK substrate.

TABLE 1: Material constants used in the J–C plasticity model [24, 25].

Material property	Sn	PEEK
Density, ρ (kg/m^3)	7280	1304
Young's modulus, E (GPa)	41	1.97
Poisson's ratio, ν	0.36	0.3
Thermal conductivity, k (W/m.K)	60	0.295
Specific heat, C_p (J/kg.K)	227	2180
Initial flow stress, A (MPa)	41	132
Pre-exponential factor, B (MPa)	276	10
Work hardening exponent, n	0.71	1.2
Strain rate factor, C	0.0766	0.034
Thermal softening exponent, m	0.73	0.7
Melting temperature, T_m (K)	505	616
Reference temperature, T_o (K)	298	298
Reference strain rate, $\dot{\varepsilon}_0$	5×10^{-4}	10^{-4}

The numerical modeling was solved using a commercial explicit finite element (FE) package (*ABAQUS 2024*) using the *Lagrangian method* under the following assumptions:

- The Sn particle is spherical with a diameter of 25 μm.
- The viscoelastic behavior of the substrate is neglected.
- The particle impact process is adiabatic, and total energy is conserved during impact.

Figs. 2c - e present the results of the simulation, showing the equivalent plastic strain (PEEQ), von Mises stress, and temperature distribution, respectively, at 60 ns after the impact. As shown in Fig. 2c, the Sn particle effectively impinged into the PEEK substrate, inducing localized plastic deformation in both the particle and the substrate. This deformation behavior reflects the high-velocity impact conditions characteristic of CS processing and confirms the particle's ability to mechanically anchor (i.e., mechanical interlocking) into the softened polymer surface during deposition. The plastic strain distribution shown in Fig. 2c further confirmed the development of localized deformation during impact, with the highest strain concentrated at the particle–substrate interface, particularly near the leading edge of the Sn particle. This strain localization is consistent with the high-stress gradients (Fig. 2d) generated during high-velocity particle impingement. The elevated temperature at the particle–substrate interface (see Fig. 2e) further reduces the flow stress of both materials, promoting additional plastic deformation. Such thermomechanical coupling is characteristic of CS impact events and plays a critical role in enabling particle embedding and interfacial bonding during deposition. Notably, the particle temperature remained below the melting point of Sn (~ 232°C = 505K [16]), confirming that the impact event occurred entirely within the solid-state processing regime. Fig. 2f illustrates the plastic strain evolution at 15 ns, 30 ns, and 45 ns, demonstrating the progressive plastic deformation of both Sn and PEEK over time. This increasing deformation promotes intimate particle–substrate contact and facilitates the development of strong interfacial bonding essential for forming a continuous conductive coating. Collectively, the modeling results confirmed the successful bonding and mechanical interlocking of the Sn particle with the PEEK substrate, and further justified the selection of the CS processing parameters (i.e., gas temperature of 300^oC, and pressure of 0.5 MPa) for experimental studies.

3.2. Electrical and microstructural performance

Fig. 3a shows the variation in electrical resistance across composite powders with different regolith weight ratios. The electrical resistance was measured between the two ends of the specimens (i.e., 30 mm in length) using the two-point probe method. Even though the particles were able to impinge into the PEEK polymer (see Fig. 4a), no measurable electrical conductivity was observed in the samples produced with a single spray pass. This behavior is attributed to the discontinuity of the deposited Sn layer, which disrupts electron pathways and inhibits current flow, as confirmed by the microstructural analysis shown in Fig. 4a. This finding is further supported by the porosity analysis in Fig. 3b, where the single-pass coatings exhibited the highest porosity levels (~60%), indicating a lack of continuous metallic connectivity essential for charge transport. The high porosity is likely due to polymer jetting caused by the high-speed impact of particles, as also indicated by the FEA simulations (see Fig. 2).

Notably, electrical conductivity was achieved in samples produced with two and three spray passes (see Fig. 3a), indicating the formation of a continuous metallic network that facilitates efficient electron transport, as presented in Fig. 4b. Additionally, the porosity calculations in Fig. 3b further supports this finding, revealing a significant reduction in porosity for samples with multiple spray passes. This improvement is attributed to the tamping effect of the successive layers, which enhances material consolidation. Furthermore, the electrical resistance increased with the rising proportion of lunar regolith in the composite mixture, with loss of conductivity occurring at regolith contents exceeding 60 wt% for two spray passes and 70 wt% for three spray passes (see Fig. 3a).

In addition to resistance measurements, the electrical conductivity of specimens with different spray passes was calculated

Downloaded from asmedigitalcollection.asme.org/MSEC/proceedings-pdf/MSEC2026/89633/V002T05A011/7651958/v002t05a011-msec2026-182587.pdf by Purdue University at West Lafayette, Yuseop Sim on 05 November 2026

Copyright © 2026 by ASME

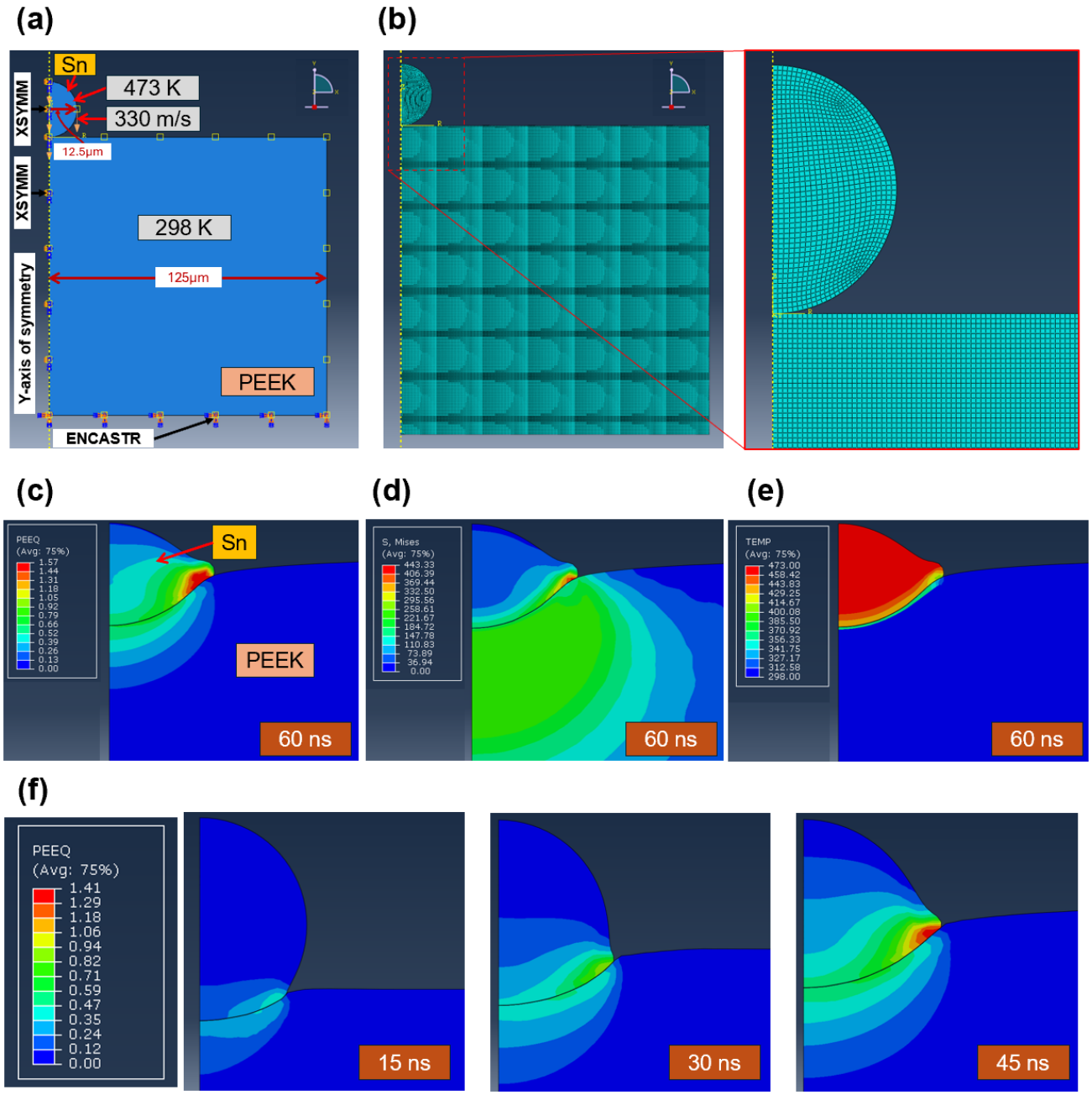


FIGURE 2: Modeling of single-particle impact: (a) Computational domain with boundary conditions; (b) Mesh of the computational domain; (c) Equivalent plastic strain (PEEQ), (d) Von Mises stress (MPa) and (e) temperature distribution (K) at 60 ns; (f) Progressive evaluation of plastic strain (PEEQ) over time at 15 ns, 30 ns, and 45 ns.

using Eq. 2, where σ' is conductivity, ρ' is resistivity, L is coating length, R is resistance, and $A' = w \times t$ is the cross-sectional area, with w and t denoting the coating width and thickness, respectively. The coating thickness was determined from the cross-sectional SEM images shown in Fig. 4c. Notably, no noticeable porosity was observed in the cross-sections, particularly for specimens with two and three spray passes, confirming successful CS deposition and effective particle consolidation. These observations highlight the dense and uniform nature of the coatings, which directly contributes to the improved electrical conductivity and mechanical integrity of the deposited layers.

Fig. 3c shows the variations in conductivity and coating thickness with different numbers of spray passes. A notable increase in conductivity was observed from two to three spray passes ($\sim$ 120%). This improvement is primarily attributed to (i) greater coating thickness, which promotes enhanced particle interconnectivity, and (ii) reduced porosity, resulting in more continuous and efficient electrical pathways throughout the coating. Specifically, the coating thickness increased with the number of spray passes, from $\sim$ 20μm after one pass to $\sim$ 40μm after three passes (Fig. 3c). The increase in coating thickness results from the continued buildup of the plastically deformed Sn

Copyright © 2026 by ASME

Downloaded from asmedigitalcollection.asme.org/MSEC/proceedings-pdf/MSEC2026/89633/V002T05A011/7651958/v002t05a011-msec2026-182587.pdf by Purdue University at West Lafayette, Yuseop Sim on 05 November 2026

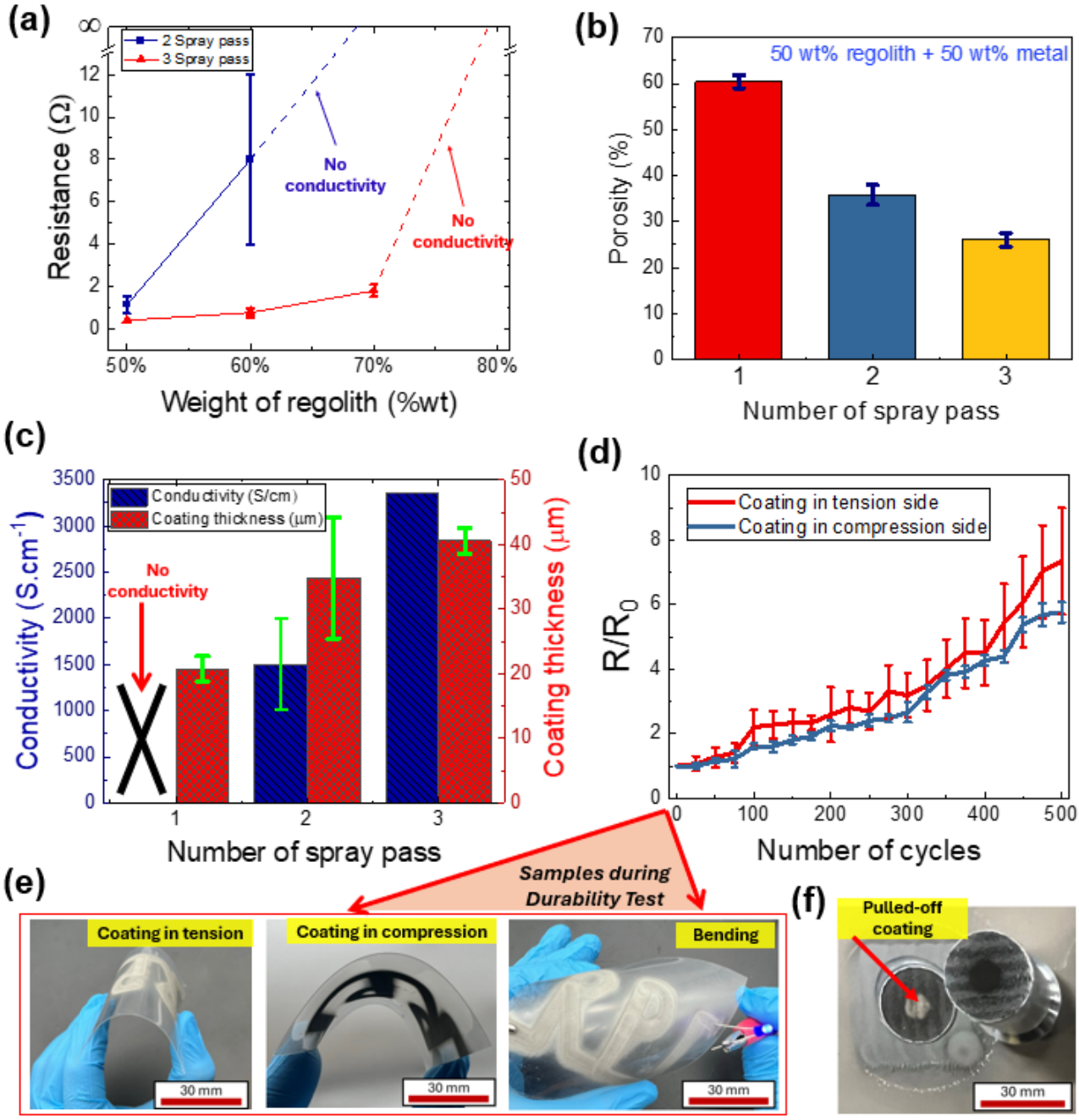


FIGURE 3: (a) Change of resistance with number of spray pass and weight of regolith (%wt); (b) Variation of surface porosity with the number of spray pass; (c) Change of conductivity and coating thickness with number of spray pass; (d) Durability test; (e) Coated samples during durability test; and (f) Pull-off adhesion strength test. (For all experiments, three specimens were used to ensure statistical validity, with flexural tests repeated three times on the same specimen).

layer during successive spray passes, along with the impingement of regolith ceramic particles into the PEEK substrate. This impingement, driven by particle kinetic energy, induces a shot-peening-like tamping effect [26], which further enhances coating consolidation (see Fig. 4c). Consequently, according to Eq. 3, the increased coating thickness results in reduced resistance and, in turn, higher conductivity. These findings are supported by the observed variations in coating thickness and porosity in Figs. 3b–c, as well as the microstructural features shown in Figs. 4b–c.

$$\sigma' = \frac{1}{\rho'} = \frac{L}{RA'} = \frac{L}{R(w \times t)} \tag{2}$$

$$R = \rho' \times \frac{L}{A'} \tag{3}$$

The EDX elemental maps of both the surface (Fig. 4d) and cross-section (Fig. 4e) also confirmed the successful deposition and distribution of the key composite powder constituents. The presence of distinct elemental signatures from both the metallic

Copyright © 2026 by ASME

Downloaded from asmedigitalcollection.asme.org/MSEC/proceedings-pdf/MSEC2026/89633/V002T05A011/7651958/v002t05a011-msec2026-182587.pdf by Purdue University at West Lafayette, Yuseop Sim on 05 November 2026

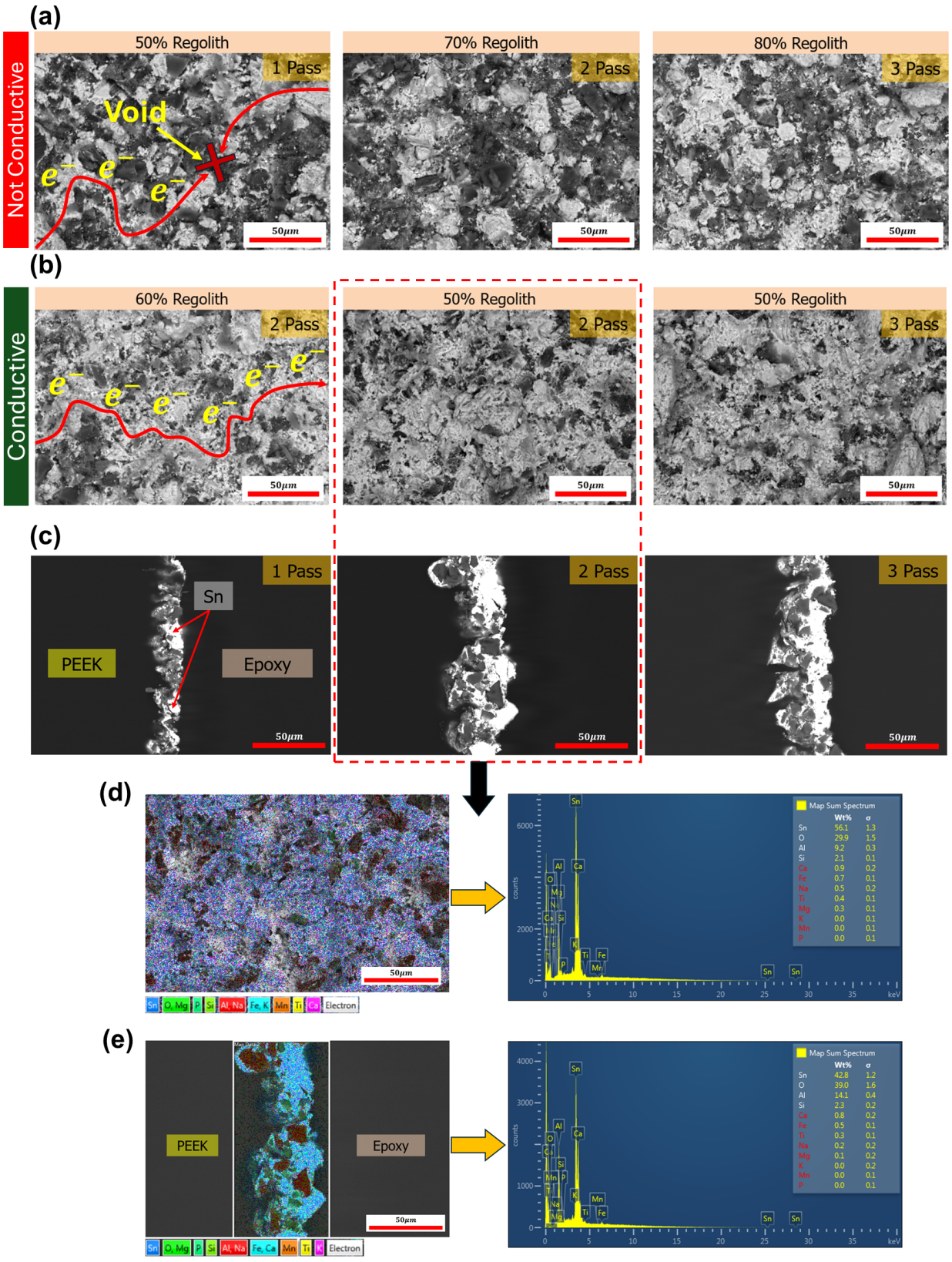


FIGURE 4: Microstructural characterization of the fabricated coatings: (a) Surface SEM images of non-conductive coatings with regolith concentrations of 50 wt% (1 pass), 70 wt% (2 passes), and 80 wt% (3 passes); (b) Surface SEM images of conductive coatings with 60 wt% (2 passes), 50 wt% (2 passes), and 50 wt% (3 passes); (c) Cross-sectional SEM images of 50 wt% regolith + 50 wt% metal coatings at varying spray passes; (d) EDX elemental maps; and (e) EDX spectra of the surface and cross-section for the 50 wt% regolith + 50 wt% metal coating (2 passes).

Copyright © 2026 by ASME

Downloaded from asmedigitalcollection.asme.org/MSEC/proceedings-pdf/MSEC2026/89633/V002T05A011/7651958/v002t05a011-msec2026-182587.pdf by Purdue University at West Lafayette, Yuseop Sim on 05 November 2026

(Sn) and ceramic (regolith) phases indicates effective deposition and strong interfacial bonding within the coating, validating the formation of a well-integrated composite coatings on the PEEK substrate. Collectively, these results demonstrate the feasibility of producing conductive, mechanically robust regolith-based coatings on polymeric substrates through programmable CS processing, enabling the development of multifunctional surfaces for in-space electronic and structural applications.

3.3. Durability and adhesion strength

The mechanical robustness and adhesion integrity of the cold-sprayed lunar regolith composite coatings were evaluated to assess their durability under operational stresses. In this context, the as-CS deposited (single pass) PET specimen (Fig. 1h) was subjected to cyclic bending deformation at an angle of $\sim 60^{\circ}$ for 500 cycles. The relative (normalized) resistance change (R/R_0) was recorded throughout the test to quantify the electrical stability of the coatings. This measurement also provided insight into the durability of the conductive network and its ability to maintain performance under repeated deformation.

Fig. 3d presents the variation of R/R_0 of the coating as a function of bending cycles, comparing the coating surfaces located on the tension and compression sides during cyclic deformation. Fig. 3e (left and middle panels) illustrates the deformation modes applied during testing, corresponding to tensile and compressive bending conditions. In both cases, the coatings exhibited a gradual increase in resistance with increasing cycle count, indicating such degradation of the electrical pathways. This behavior is likely attributed to microcrack initiation and/or interfacial fatigue within the coating–substrate system. Notably, the rate of resistance increase is higher on the tension side, where tensile stresses lead to greater disruption of the conductive network. In contrast, the compression side showed a more stable resistance response, suggesting that compressive loading helps preserve particle contact and maintain electrical continuity.

Notably, the overall resistance remained below 100 Ω even after 500 bending cycles, indicating electrical stability of conductive pathways within the coating, despite repeated mechanical deformation (see Fig. 3e, right panel). This durability further supports the coatings' potential for reliable use in flexible electronic. Given that the electrical resistance exhibited clear sensitivity to mechanical deformation (i.e., $R/R_0 \approx 8$ for the tension side and $R/R_0 \approx 6$ for the compression side), the system demonstrates strong potential for use as a strain gauge in deformation- or stress-sensing applications.

The adhesion strength was quantified using a pull-off adhesion tester (*Elcometer 510*) following the ASTM D4541 standard [18]. The as-sprayed PEEK sample was tested for the pull-off adhesion strength test, with each test repeated three times to ensure statistical validity and reproducibility. Circular aluminum dollies (14-mm diameter) were bonded to the coating surfaces using an epoxy adhesive (*3M 460*) and allowed to cure for 24 hours at room temperature before testing. A constant detachment load rate of 2 $MPa.s^{-1}$ was applied until the dolly separated from the surface (see Fig. 3f). The average adhesion strength was measured as 7.71 ± 0.65 MPa, demonstrating competitive performance compared to values reported in previous studies on polymer metallization [27].

4. CONCLUSION

This work investigated the cold spray (CS) deposition of lunar regolith–based composite powders to develop electrically conductive surfaces, demonstrating their promise for in-space electronics manufacturing. To this end, composite powders consisting of lunar regolith simulant (LHS-1D) and metallic additives (Sn + Al_2O_3) were engineered as solid-state feedstock for the CS process and subsequently deposited onto polymer substrates (PEEK) at varying weight ratios under terrestrial conditions. The principal outcomes of this work are summarized as follows:

- FE modeling confirmed effective particle-substrate bonding and justified the selected CS parameters (i.e., gas temperature and pressure).
- Conductive coatings were successfully deposited on PEEK, PET, and 3D-printed TPU using the CS process.
- Increasing the number of spray passes enhanced coating conductivity from 1500 $S.cm^{-1}$ to 3300.cm^{-1}.
- Coating thickness increased from ~20 μm to ~40 μm, with additional spray passes.
- The coating exhibited promising mechanical durability, retaining conductivity (< 100 Ω) after 500 bending cycles (i.e., $R/R_0 \approx 8$ in tension and $R/R_0 \approx 6$ in compression).
- The deposited Coatings exhibited strong adhesion strengths ranging from 7.30 to 8.46 MPa.

Despite these promising results under terrestrial conditions and the potential of CSAM in space conditions [13], future work should focus on evaluating (i) the synthesis and optimization of composite feedstock powders and (ii) the CS process and coating performance in simulated lunar environments, including vacuum conditions, reduced gravity, extreme temperature fluctuation effects. Such investigations would provide a more comprehensive understanding of the feasibility of regolith-based conductive coatings for in-space electronics manufacturing.

ACKNOWLEDGMENTS

The authors acknowledge the internal funding provided by the Department of Mechanical, Aerospace, and Nuclear Engineering (MANE) Department at Rensselaer Polytechnic Institute.

REFERENCES

[1] Rasera, JN, Cilliers, JJ, Lamamy, JA and Hadler, K. "The beneficiation of lunar regolith for space resource utilisation: A review." *Planetary and Space Science* Vol. 186 (2020): p. 104879.

[2] Esho, Adeola Ona-Olapo, Iluyomade, Tosin Daniel, Olatunde, T Michael and Igbinenikaro, Osayi Philip. "Next-generation materials for space electronics: A conceptual review." *Open Access Research Journal of Engineering and Technology* Vol. 6 No. 02 (2024): pp. 051–062.

[3] Lab, Exolith. "LHS-1D Lunar Highlands Simulant Specification Sheet." https://cdn.shopify.com/s/files/1/0398/9268/0862/files/LHS-1D_SPEC_SHEET_DEC_2023.pdf?v=1745852728 (2023). Accessed: 2025-11-04.

Copyright © 2026 by ASME

Downloaded from asmedigitalcollection.asme.org/MSEC/proceedings-pdf/MSEC2026/89633/V002T05A011/7651958/v002t05a011-msec2026-182587.pdf by Purdue University at West Lafayette, Yuseop Sim on 05 November 2026

[4] Akisheva, Yulia, Gourinat, Yves, Guatelli, Susanna, Dossat, Cédric, Robin-Chabanne, Steven, Varotsou, Athina, Cowley, Aidan and Makaya, Advenit. "Regolith-based lunar habitats: an engineering approach to radiation shielding." *CEAS Space Journal* Vol. 16 No. 6 (2024): pp. 667–676.

[5] Gupta, Ayushi, Sahu, Sonika, Ukey, Piyush, Kumar, Atish, Gupta, Vivek, Sachdeva, Anish and Kumar, Narendra. "Additive Manufacturing for Space Applications: A Review of Processes, Properties, and Prospects." *Acta Astronautica* (2025).

[6] Kenny, Vinay, Bapat, Salil and Malshe, Ajay P. "Exploring the feasibility of processing Inconel-718 and highland regolith composite using laser-assisted powder bed fusion." *Procedia CIRP* Vol. 121 (2024): pp. 198–203.

[7] Das, Pial, Umerov, Emil, Dyrstad-Cincotta, Nicholas, Rimon, Md Touhidul Islam, Mazurkivich, Matthew, Rengifo, Sara, Scott, William, Wang, Yachao and Roy, Sougata. "Exploring the erosion resistance of Al6061 metal matrix composite fabricated via additive manufacturing for future lunar exploration." *Progress in Additive Manufacturing* (2025): pp. 1–17.

[8] Wang, Tongcai, Gu, Guangshuai, Zhang, Rihan, Cui, Qianshun and Wang, Gong. "Additive Manufacturing of Lunar Regolith via Resin-Based Binder and Material Extrusion Method for High-Performance In-Situ Manufacturing on the Moon." *Additive Manufacturing Frontiers* (2025): p. 200233.

[9] Johnson, Francis S, Carroll, James M and Evans, Dallas E. "Vacuum measurements on the lunar surface." *Journal of Vacuum Science and Technology* Vol. 9 No. 1 (1972): pp. 450–456.

[10] National Aeronautics and Space Administration (NASA). "Weather on the Moon." https://science.nasa.gov/moon/weather-on-the-moon/ (2025). Accessed: 2025-07-31; page last updated June 25, 2025.

[11] Reitz, B, Lotz, C, Gerdes, N, Linke, S, Olsen, E, Pflieger, K, Sohrt, S, Ernst, M, Taschner, P, Neumann, J et al. "Additive manufacturing under lunar gravity and microgravity." *Microgravity Science and Technology* Vol. 33 No. 2 (2021): p. 25.

[12] Azami, Mohammad, Kazemi, Zahra, Moazen, Sare, Dubé, Martine, Potvin, Marie-Josée and Skonieczny, Krzysztof. "A comprehensive review of lunar-based manufacturing and construction." *Progress in Aerospace Sciences* Vol. 150 (2024): p. 101045.

[13] Rahman, Sazedur and Akin, Semih. "Cold spray deposition of lunar regolith on polymeric substrates: A pathway toward in-situ resource utilization on the Moon." *Surfaces and Interfaces* (2025): p. 108224.

[14] Kalácska, Ádám, Parmentier, Victor, De Baets, Patrick and Kalácska, Gábor. "Wear investigation of PTFE, PEEK and UHMWPE-based reciprocating shaft seal materials with lunar/Martian regolith simulants." *Wear* (2025): p. 205791.

[15] Azami, Mohammad, Aubin-Fournier, Pierre-Lucas and Skonieczny, Krzysztof. "Enhancing economical lunar-based manufacturing by incorporating lunar regolith into polyether–ether–ketone (PEEK): material development, additive manufacturing, and characterization." *Progress in Additive Manufacturing* (2025): pp. 1–7.

[16] Akin, Semih, Lee, Seungjun, Jo, Seunghwan, Ruzgar, Duygu Gazioglu, Subramaniam, Karthick, Tsai, Jung-Ting and Jun, Martin Byung-Guk. "Cold spray-based rapid and scalable production of printed flexible electronics." *Additive Manufacturing* Vol. 60 (2022): p. 103244.

[17] Champagne, V and Helfritch, D. *International Materials Reviews* Vol. 61 No. 7 (2016): pp. 437–455.

[18] Lee, J, Akin, S, Walsh, JR, Jun, MBG, Lee, H and Shin, YC. "A Nitinol structure with functionally gradient pure titanium layers and hydroxyapatite over-coating for orthopedic implant applications." *Progress in Additive Manufacturing* Vol. 9 No. 4 (2024): pp. 1025–1038.

[19] Tsai, Jung-Ting, Akin, Semih, Bahr, David F and Jun, Martin Byung-Guk. "A predictive modeling approach for cold spray metallization on polymers." *Surface and Coatings Technology* Vol. 483 (2024): p. 130711.

[20] Behera, Ajay Kumar, Mantry, Sisir, Roy, Sudesna and Pati, Soobhankar. "Numerical Investigation of the Metal–Ceramic Coating Mechanism Through Cold Spray." *Journal of Thermal Spray Technology* (2025): pp. 1–23.

[21] Feng, Po-Lun, Duran, Salih, Blassino, Adolfo, Nault, Isaac, Müftü, Sinan and Nutt, Steven. "Cold Spray Niobium Metallization of Carbon Fiber Reinforced Thermoset Composite enabled by Hybrid Bond Layer." *Materials Science and Engineering: A* (2025): p. 148409.

[22] Adaan-Nyiak, Moses A and Tiamiyu, Ahmed A. "Recent advances on bonding mechanism in cold spray process: A review of single-particle impact methods." *Journal of Materials Research* Vol. 38 No. 1 (2023): pp. 69–95.

[23] Gabor, Theodore, Akin, Semih and Jun, Martin Byung-Guk. "Numerical studies on cold spray gas dynamics and powder flow in circular and rectangular nozzles." *Journal of Manufacturing Processes* Vol. 114 (2024): pp. 232–246.

[24] Vafaeenezhad, H, Seyedein, SH, Aboutalebi, MR and Eivani, AR. "Incorporating the Johnson–Cook constitutive model and a soft computational approach for predicting the high-temperature flow behavior of Sn-5Sb solder alloy: a comparative study for processing map development." *Journal of Electronic Materials* Vol. 46 No. 1 (2017): pp. 467–477.

[25] Kang, Jianfeng, Zheng, Jibao, Hui, Yijun and Li, Dichen. "Mechanical properties of 3D-printed PEEK/HA composite filaments." *Polymers* Vol. 14 No. 20 (2022): p. 4293.

[26] Okuniewski, Wojciech, Walczak, Mariusz and Szala, Mirosław. "Effects of shot peening and electropolishing treatment on the properties of additively and conventionally manufactured Ti6Al4V alloy: A review." *Materials* Vol. 17 No. 4 (2024): p. 934.

[27] Chen, Siying, Zhou, Fengfeng, Reggetz, Bailley N, Lee, Eun Gyung, Virji, M Abbas, Afshari, Aliakbar, Jun, Martin Byung-Guk and Akin, Semih. "Polymer metallization via cold spray: an investigation into the effects of particle hardness and morphology." *Manufacturing Letters* Vol. 44 (2025): pp. 325–331.

Downloaded from asmedigitalcollection.asme.org/MSEC/proceedings-pdf/MSEC2026/89633/V002T05A011/7651958/v002t05a011-msec2026-182587.pdf by Purdue University at West Lafayette, Yuseop Sim on 05 November 2026

Copyright © 2026 by ASME